

Dressed Active Particles in Spherical Crystals

Zhenwei Yao

*Department of Physics and Astronomy, and Institute of Natural Sciences,
Shanghai Jiao Tong University, Shanghai 200240 China*

We investigate the dynamics of an active particle in two-dimensional spherical crystals, which provide an ideal environment to illustrate the interplay of active particle and crystallographic defects. A moving active particle is observed to be surrounded by localized topological defects, becoming a dressed active particle. Such a physical picture characterizes both the lattice distortion around the moving particle and the healing of the distorted lattice in its trajectory. We find that the dynamical behaviors of an active particle in both random and ballistic motions uniformly conform to this featured scenario, whether the particle is initially a defect or not. We further observe that the defect pattern around a dressed ballistic active particle randomly oscillates between two well-defined wing-like defect motifs regardless of its speed. The established physical picture of dressed active particles in this work partially deciphers the complexity of the intriguing nonequilibrium behaviors in active crystals, and opens the promising possibility of introducing the activity to engineer defects, which has strong connections with the design of materials.

I. INTRODUCTION

Ubiquitous nonequilibrium condensed matter systems exhibit a wealth of intriguing properties not found in the equilibrium zone. [1–4] From highly coherent collective motions in moving animals, [5, 6] bacterial suspensions, [7, 8] living cells, [9–11] and living liquid crystals [12] to emergent ordered structures developed in granular matters in vibration, [13, 14] colloids, [7, 15] nanoparticles, [16] soft particles, [17] and active spinners, [18, 19] these seemingly distinct systems have a unifying characteristic that they are composed of self-driven active units and have been known as active matters or living matters. [1, 3, 20] A large variety of these nonequilibrium properties can be well rationalized in a unified physical model by endowing interacting constituent particles with activity. [3, 20, 21] Through various mechanisms such as external electric or magnetic field, [22] light, [23–25] mechanical vibration, [13] chemical reaction, [16, 26] and biological activity, [27] *etc.*, the energy input through individual active particles drives the system out of equilibrium and produces various ordered dynamic states and even biomimetic behaviors. [3] Recent studies in both polar [28–30] and apolar [31] active systems, depending on whether the constituent particles have a head and a tail, have shown the crucial role of singular points known as topological defects [32] in organizing active particles to move in a highly coherent fashion. Remarkably, the combination of topological defects and activity can produce a myriad of dynamical states as demonstrated in a recent experiment, where tunable periodic oscillation of the defects in the active nematic vesicle has been directly observed. [33] These studies suggest that the complexity in the intriguing nonequilibrium behaviors arising from activity may be characterized by the dynamics of a few topological defects. It is therefore of interest to study the interplay of active particle and topological defects to enhance our understanding of the activity induced complex dynamics in active matters.

Spherical crystal is an ideal model system to study

the physics of topological defects. [34–36] In a spherical crystal, particles are confined on the surface of sphere to constitute a two-dimensional crystal lattice. Topological defects are inevitable in two-dimensional crystalline order confined on spherical geometry due to the topological constraint. [37] These defects provide the unique opportunity to investigate the interplay of activity and topological defects. Disclinations are the elementary topological defects in two-dimensional hexagonal lattices. [38] An n -fold disclination is a vertex whose coordination number $n \neq 6$. A topological charge of $q = 6 - n$ can be assigned to an n -fold disclination. Note that one should distinguish between topological charge and electric charge associated with a particle. All the particles in spherical crystal are electrically charged, while a particle is topologically charged if its coordination number is deviated from six. According to the elasticity theory of topological defects, disclinations of the same sign repel and unlike signs attract. [36] Euler's theorem states that the total topological charge in any spherical crystal is 12. [37] It is important to note that a particle in the spherical crystal can be assigned an active force, becoming an active particle. A particle can also be a disclination if its coordination number is deviated from 6. The double role of a particle in the spherical crystal opens the possibility of moving a disclination by assigning activity on it.

In this work, we introduce an active particle in spherical crystal, where topological defects are inevitable. A spherical crystal can be experimentally realized by confining electrically charged particles on sphere, which can spontaneously form a hexagonal lattice with scattered disclinations under the Coulomb potential. [35] We consider dynamics of the particles in the overdamped regime described by the Langevin equation. The objective of this work is to understand the activity induced nonequilibrium physics in terms of the elements of topological defects. We prepare the initial state of the spherical crystal with the simplest configuration of evenly distributed 12 isolated 5-fold disclinations. We first numerically observe

the intermediate hexatic phase in the noise driven melting of the spherical crystal. It is comparable with the scenario of the dislocation-mediated melting theory of two-dimensional crystals proposed by Kosterlitz, Thouless, Halperin, Nelson and Young (KTHNY theory), suggesting the reliability of our simulations. [39–43]

At a low level of noise below the melting point, we impose an active force on a particle in the spherical crystal and track its dynamics and the resulting adjacent lattice distortion. Such a lattice distortion is well represented by the underlying topological defect structure via the triangulation of the particles on sphere. Extensive simulations show that an active particle always carries disclinations around it in both random and ballistic motions, whether the particle is initially a disclination or not. We name such a compound structure of active particle and surrounding disclinations as a dressed active particle. For an initially disclination active particle, we numerically observe its splitting into an isolated disclination and a dressed active particle with zero topological charge. The topological charge of the active particle remains in the original site in the form of an isolated disclination, avoiding a global structural transformation to move a topological charge in crystal. The distorted lattice in the trajectory of a self-propelled active particle is observed to restore the hexagonal configuration. Few neutral quadrupoles may be excited in the trajectory of a moving particle to release the slight local residue stress. Notably, simulations show that when an active particle switches from the random to the ballistic motion, the originally swelled surrounding defect cluster shrinks in the direction of the motion, leading to two types of wing-like defect motifs. We further observe the random oscillation of a dressed active particle between these two defect motifs regardless of the speed of the motion. The revealed uniform physical picture of dressed active particle in this work has implications for the engineering of defects in materials design, and it also provides the basis for further investigation of the statistical behaviors of active particles.

II. MODEL

We construct the initial state of spherical crystal composed of point particles from a regular icosahedron with 12 vertices and 20 triangles. In each triangle, we first introduce $n - 1$ particles on each bond to equally divide the bond into n segments. The original triangle is divided by connecting any two particles at the same height relative to their opposite side. Extra particles are placed at the intersect of these connecting lines. The total number of particles in the triangulated icosahedron is $N = 10(n^2 - 1) + 12$. For a spherical crystal of N particles and area A_0 , the lattice spacing $a = \sqrt{2A_0/(\sqrt{3}N)}$. By mapping the vertices to a sphere whose center coincides with the center of the icosahedron, we obtain a spheri-

cal crystal with 12 evenly distributed 5-fold disclinations. Such a spherical crystal has a minimum number of defects allowed by the topological constraint, and provides an ideal environment to study the interplay of active particles and isolated defects. Note that in terms of the Caspar–Klug construction for hexagonal and triangular lattices on sphere, the lattice of our constructed spherical crystal has the coordinates of (p, q) with $q = 0$. [44] p and q are the numbers of steps between successive pentagons on a spherical crystal. We will show later that the physical picture of dressed active particle does not rely on the specific value of p and q .

We work in the regime of overdamped dynamics. In the hydrodynamics of small size particles where the Reynolds number is sufficiently small, the inertial effect can be ignored. The motion of the particles conforms to the overdamped Langevin equation which reads: [45]

$$\dot{\vec{r}}_i = \vec{P}_T[\vec{r}_i(t), f\hat{u}_i(t) + \sum_j \vec{F}_{ij} + A\vec{\xi}_i(t)], \quad (1)$$

where \vec{r}_i is the position of the particle labeled i ($i = 1, 2, 3 \dots N$). The projection operator $\vec{P}_T[\vec{r}_i(t), \vec{a}] = \vec{a} - (\hat{r}_i(t) \cdot \vec{a})\hat{r}_i(t)$. $\eta\vec{r}_i$ is the viscous force on the particle i . The three terms in the second expression in the square bracket in Eq.(1) represent three contributions to the forces on the particles. $f\hat{u}_i(t)$ is the self-propulsion force of magnitude f and temporally varying direction $\hat{u}_i(t)$. About the orientation $\hat{u}_i(t)$ of the active force, we consider the following cases: (1) the orientation of $\hat{u}_i(t)$ is generated from the uniform distribution in the interval of $[0, 2\pi]$; (2) ballistic motion, where $\hat{u}_i(t)$ is a constant; (3) the orientation of $\hat{u}_i(t)$ changes by angle θ in each time step, which conforms to the Gaussian distribution with mean zero and variance $\Delta\theta^2$. For simplicity, here we do not include the time-correlation in the evolution of $\hat{u}_i(t)$. The time-correlation of noise is important in understanding glassy dynamics. [46] $\vec{F}_{ij} = -\nabla V_{ij}$ is the Coulomb force on the particle i exerted by the particle j . $V_{ij} = \beta \frac{1}{|\vec{r}_i - \vec{r}_j|}$. The last term $A\vec{\xi}_i(t)$ models the random force on the particle i . A is the amplitude of the force, and $\vec{\xi}_i(t)$ is a delta-correlated Gaussian noise. $\langle \vec{\xi}_i(t) \rangle = 0$. $\langle \xi_{i,\alpha}(t)\xi_{j,\beta}(t) \rangle = \delta_{ij}\delta_{\alpha\beta}$, where α and β denote the components of the vector $\vec{\xi}_i(t)$ in the associated tangent plane at \vec{r}_i . $\vec{\xi}_i$ is in the tangent plane at \vec{r}_i on sphere. Note that the noise term $\xi(t)dt$ in Eq.(1) is interpreted in the frame of stochastic calculus. [47, 48] Specifically, the integration is over the standard Wiener process $\{W(t), t \geq 0\}$, where $\Delta W = W(t + \Delta t) - W(t)$ constitutes independent increments of the random variable $W(t)$. Note that the electrostatic interaction between two charged particles whose size is much smaller than their separation dominates over their hydrodynamic interaction [49]. We therefore do not consider the hydrodynamic interaction between particles in the model. We measure length in the unit of the lattice spacing a , energy in the unit of $\epsilon_0 = \beta/a$, time in the unit of $\tau = \eta a^3/\beta$, and force in the unit of ϵ_0/a .

From Eq.(1), we can construct the trajectory of the particles from

$$\vec{r}_i(t + \Delta t) = \vec{r}_i(t) + \dot{\vec{r}}_i \Delta t. \quad (2)$$

In numerically solving the Langevin equation, we choose the time step $\Delta t = 10^{-3}\tau$. For convenience in simulations, the magnitude A of the noise is expressed in terms of Γa , where Γ is a fraction of unity. $\eta \frac{\Gamma a}{\Delta t} = A$. In terms of the units for energy (ϵ_0) and time (τ), $A = \Gamma \epsilon_0 \tau / (a \Delta t)$. From Eqs.(1) and (2), we obtain the dimensionless discretized Langevin equation

$$\frac{\tilde{r}_i(\tilde{t} + \Delta \tilde{t}) - \tilde{r}_i(\tilde{t})}{\Delta \tilde{t}} = \vec{F}_T[\tilde{r}_i(\tilde{t})], \frac{\tilde{f}}{\Delta \tilde{t}} \hat{u}_i(\tilde{t}) + \sum_j \tilde{F}_{ij} + \frac{\Gamma}{\Delta \tilde{t}} \tilde{\xi}_i(\tilde{t}), \quad (3)$$

where all the quantities are dimensionless. $\tilde{t} = t/\tau$. $\tilde{r} = \vec{r}/a$. $\tilde{F} = \vec{F}a/\epsilon_0$. The activity of the particles is controlled by $\tilde{f}a$, which is a fraction of the lattice spacing a during a time step Δt . $\tilde{f} = f\Delta t/(\eta a)$. It is important to point out that the strength of noise and active force is characterized by Γa and $\tilde{f}a$, respectively, which are fractions of the lattice spacing a . The resulting factor of $\sqrt{\Delta t}$ appearing in the integration of the standard Wiener process is absorbed in these two dimensionless quantities. [47] In this way, the strength of both noise and active force is well controlled in simulations. The theoretical model in this work may be realized experimentally in curved colloidal crystals formed at the spherical interfaces of water and oil; [35] active forces may be introduced by making use of the coupling of magnetic colloids and controllable external magnetic field. [35]

III. RESULTS AND DISCUSSION

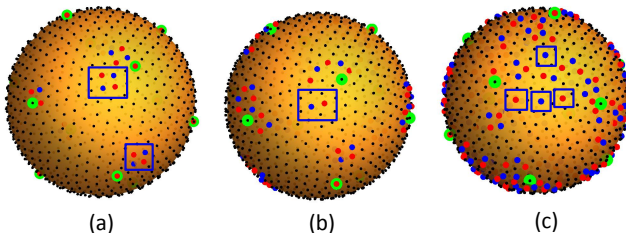


FIG. 1: Particles configurations at enhanced noise levels from $\Gamma = 0.04$ (a), $\Gamma = 0.05$ (b), to $\Gamma = 0.07$ (c) without imposing any active force. Quadrupoles [in the box in (a)], isolated dislocations [in the box in (b)] and isolated disclinations [in the box in (c)] appear in sequence with the increase of the noise strength Γ . The positions of the initial 12 5-fold disclinations are indicated by the large green dots. The red and blue dots represent 5- and 7-fold disclinations. $N = 1002$.

We first study the effect of the Gaussian noise in Eq.(3) whose strength is characterized by the parameter Γ . The expected melting of the spherical crystal at high level of noise provides a qualitative criterion to check the reliability of our simulations. Figure 1 shows the typical snapshots of the spherical crystal with the increase of the noise strength Γ . Simulations capture the splitting of quadrupoles into isolated dislocations [see Fig. 1(b)] and their further fission into isolated 5- and 7-fold disclinations [from Fig. 1(c)]. Therefore, the simulated spherical crystal system experiences the intermediate hexatic phase characterized by the proliferation of dislocations in the noise driven crystal-to-liquid phase transition. This hexatic phase has been predicted by the KTHNY theory for the melting of infinitely large two-dimensional planar crystals. [39–43] Note that MD simulations of two-dimensional melting on sphere with a repulsive r^{-12} potential also return results that are consistent with the KTHNY theory. [50] In our system, the parameter Γ that controls the step size in the random motion of the particles plays a similar role of temperature in the KTHNY theory. The appearance sequence of quadrupoles, dislocations, and disclinations with the increase of Γ is also observed in smaller spherical crystals. In the spherical crystal of 252 particles, isolated dislocations and disclinations appear at $\Gamma_{c_1} = 0.04$ and $\Gamma_{c_2} = 0.05$, respectively. Γ_{c_1} is the critical melting condition from crystal to hexatic phase, and Γ_{c_2} is that from hexatic to liquid phase. Both these critical values for Γ are smaller than those in the larger system of 1002 particles.

The size-dependence of the critical melting conditions is related to the compactness of the spherical crystal. By confining more mutually repulsive particles in a compact surface without a boundary like a sphere or a torus, the system becomes stiffer. Specifically, for N electrically charged particles with the $1/r$ -Coulomb potential confined on sphere, the energy of the system increases with N in the form of $E(N) \propto N^2/2 - 0.5510N^{3/2}$. [51] It leads to an enhanced Young's modulus of the elastic medium composed of the equilibrium hexagonal lattice. The binding energy of a dislocation pair and a disclination pair is proportional to the Young's modulus. [38] Consequently, the binding energy of the defect clusters like quadrupoles and dislocations is elevated with the increase of the number of particles. We therefore require a larger Γ to activate the proliferation of isolated dislocations and disclinations to realize the respective phase transitions.

A. Random active force

Now we tune the noise Γ to a low level below the melting point in order to highlight the dynamic features of an active particle. We introduce an active particle in the spherical crystal by imposing a random active force \tilde{f} in Eq.(3), and study its dynamics and interplay with the pre-existent disclinations. With the increase of the

magnitude of the active force, we observe that the active particle finally escapes from the initially trapped state and gains mobility when \tilde{f} exceeds some critical value $\tilde{f}_{\text{critical}}$. The value for $\tilde{f}_{\text{critical}}$ is unaffected by the noise strength Γ . For a spherical crystal of 1002 particles, $\tilde{f}_{\text{critical}} \approx 0.03$ for Γ ranging from 0.001 to 0.04. For an arbitrarily chosen trapped active particle at low Γ , whether it is a disclination or not, increasing the noise strength only induces a localized slight distortion of the crystal lattice near the trapped active particle; the maximum amount of the movement of the active particle does not exceed even one lattice spacing over up to a million time steps. Therefore, it is the active force instead of the noise that provides the drive force to propel a particle.

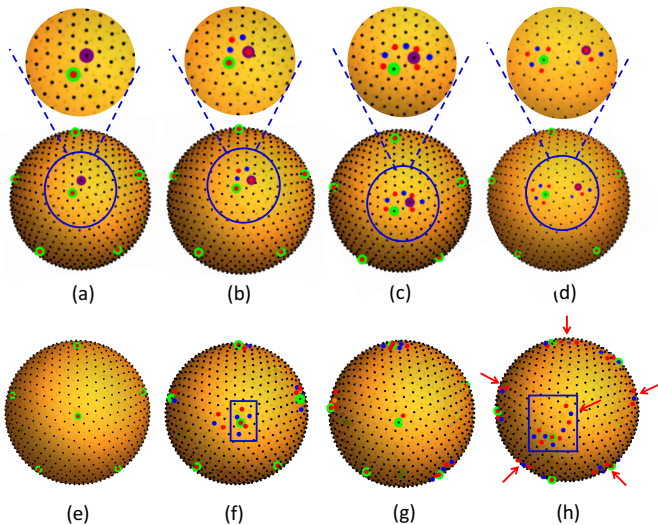


FIG. 2: Typical particles configurations to show the dynamic behaviors of active particles represented by large purple dots in (a)-(d) and large green dots in (e)-(h), respectively. The red and blue dots represent 5- and 7-fold disclinations. $\tilde{f} = 0.05$. $\Gamma = 0.001$ (a-d) and 0.002 (e-h). $N = 1002$. $t/\Delta t = 1100, 2100, 4100, 8100$ from (a)-(d). $t/\Delta t = 22000, 24000, 28000, 44000$ from (e)-(h).

Figures 2(a)-2(d) show the interaction of the active particle (the large purple dot) initially near an isolated 5-fold disclination (the large green dot) [see Fig. 2(a)]. We numerically observe that the active particle induces topological charges when it approaches the isolated disclination, creating a defect cluster with total topological charge +1 [see Fig. 2(b)]. This phenomenon can be understood in the following way. According to the elasticity theory of topological defects, disclinations of the same sign repel and unlike signs attract. A pair of positive and negative disclinations constitute a dislocation which is analogous to an electric dipole. An isolated disclination can induce the formation of dislocations around it. The total topological charge in this process must be invariant as a topological constraint. [38] On the other hand, it costs energy to create defects in crystal. Around an isolated disclination, when the reduction of the energy due

to the attraction of the disclination and dislocation(s) exceeds the energy required to create dislocation(s), the isolated disclination becomes a cluster of defects. The transformation of an isolated disclination into a linear defect structure called scar has been experimentally observed in spherical crystal with the increase of the sphere radius. [36] A scar is a defect string of alternating 5-fold and 7-fold disclinations, but with one more 5-fold disclination. Here, we observe that an active particle can induce such a transformation without any change of the sphere size.

As shown in Fig. 2(c) and (d), the random active force later pulls the active particle away from the defect cluster. When the active particle moves in the crystalline zone among the isolated disclinations, the distorted crystalline lattice behind it is healed. While few neutral quadrupoles appear in the smaller system of $N = 252$, the trajectory of a moving particle in the larger system of $N = 1002$ is free of defects. This can be attributed to the larger Young's modulus in larger systems, which elevates the energy barrier for the formation of defects. [38] No isolated dislocations in the trajectory of a moving particle are observed; more energy is required to create a dislocation than a quadrupole according to the elasticity theory of topological defects. [38]

The restoration of the distorted crystal lattice in the trajectory behind the motion of an active particle can be attributed to the long-range repulsive interaction potential between particles. The extra free space created by a moving particle is filled up by surrounding particles under the long-range repulsive force. In order to confirm that a defect-free trajectory does not rely on the specific form of the long-range force, we perform further simulations using another long-range force in the form of $F(r) \sim 1/r$. It turns out that such a force can also support defect-free trajectories. In contrast, in the two-dimensional Lennard-Jones (L-J) crystal, where particles interact via the L-J potential, the emergent stable vacancies may impede the complete healing of the trajectory of a moving particle. [52] Simulations show that when we remove the attractive part in the L-J potential, the repulsive potential in the form of $1/r^{12}$ decays so fast that it cannot support the initially prepared crystalline order on sphere with the proliferation of defects.

To further exclude the possible influence of the dynamics of the active force on the healing of the crystalline order in the trajectory of a moving particle, we simulate cases where the reorientation of $\hat{u}_i(t)$ (the direction of the active force) is subject to a finite noise instead of being completely random. Specifically, $\hat{u}_i(t)$ rotates by angle θ in each time step, which conforms to the Gaussian distribution with mean zero and variance $\Delta\theta^2$. For both cases of $\Delta\theta = \pi/12$ and $\pi/6$, we numerically observe the restoration of the distorted lattice in the trajectory of the active particle; defects are accumulated around the moving particle. It is of interest to note that the aggregation phenomenon of defects is also observed in our recently studied size-polydispersity driven distortion of

crystal lattice. [53] It is found that an impurity particle of a wrong size in a perfect crystal induces localized defect patterns to screen the effect of the impurity particle.

Figure 2(d) shows that the crystalline order very near the active particle (in the region of a few lattice spacings) is disrupted. The active particle carries a topologically neutral defect cluster when it moves around without any contact with the pre-existent disclinations. It is essentially through this defect cluster that an active particle interacts with the isolated disclinations. Simulations show that an active particle also carries a neutral defect cluster when moving in the lattice sufficiently away from any of the isolated disclinations. Therefore, the surrounding defect cluster dressing the active particle is not caused by contact with a disclination. Such a companion defect structure reflects the intrinsic local lattice distortion near the active particle. This basic scenario of dressed active particle with surrounding topological defects is also observed in systems where the active particle is initially also an isolated disclination.

Moving an isolated disclination in crystalline order requires a global transformation of the crystal lattice due to the topological property of the disclination. [38] Take an n -fold disclination in two-dimensional hexagonal crystal for example, it can be created by removing (for $n < 6$) or adding (for $n > 6$) a $|6 - n|\pi/3$ wedge. [38] Therefore, unlike dislocations that can freely glide across a crystalline medium, the motion of isolated disclinations is usually realized through interactions with other defects or by evolving into a scar to extend itself in space. [35] It is of interest to endow an isolated disclination with activity and to observe the dynamics of the active disclination. For its dual role as an active particle and also as a disclination, here such a particle is named a disclination active particle. We impose sufficiently large active forces on the 12 isolated disclinations to mobilize them [see Fig. 2(e)]. We observe the proliferation of topological defects around the active particle and the ultimate split of the defect cluster into a scar [the 5-7-5 configuration in the left of the blue box in Fig. 2(f)] and a dressed active particle [the large green dot in the blue box in Fig. 2(f)]. This fractionalization event clearly shows that the topological feature and the activity of a particle is separable. This phenomenon is also demonstrated in Fig. 2(g), where the originally active disclination evolves into an isolated disclination (the red dot in the center) and an active particle with zero topological charge (the large green dot).

The resulting free-standing topologically charged scar [see Fig. 2(f)] from the split of the defect cluster inherits the topological charge from the original disclination active particle. Both theoretical and experimental studies on the ground state of spherical crystals show that when R/a exceeds about 5, an isolated disclination becomes a scar to lower the energy. [34–36] For the system in Fig. 2 with $N = 1002$, $R/a = 8.3$, which exceeds the critical value for the appearance of scars. Isolated disclinations are therefore metastable. Once touched by a dressed ac-

tive particle, a disclination becomes a scar as shown in Fig. 2(d) and 2(f). This observation shows that active particles can facilitate the system to conquer the energy barrier to reach a new low-energy state. In this process, the source of the required energy is from the energy input through the active particle. Once formed, a scar is observed to be anchored in the spherical crystal. The arrows in Fig. 2(h) indicate the locations of the scars or topologically charged defect clusters, all of which are close to the original sites of the isolated disclinations in Fig. 2(e). Therefore, the migration of the active particle, whether it is initially an disclination or not, can only take away a topologically neutral defect cluster. The net topological charge remains in its initial position. The origin of this phenomenon can be traced down to the topological property of the disclination that requires a global transformation of the crystal lattice to change its position.

The conversion of regularly distributed isolated disclinations into scars of distinct orientations lowers the symmetry of the system. Numerical observation of moving particles in the resulting scarred spherical crystal indicates that the basic physical picture of dressed active particle does not rely on the specific position and orientation of the pre-existent defects. It can be attributed to the fact that these defects influence the state of an active particle only when they are as close as few lattice spacings. The defect pattern around the active particle is unaffected by pre-existent defects a few lattice spacings away. Consequently, the scenario of dressed active particle is also expected in the less symmetric lattices with nonzero q or $p \neq q$ in comparison with those of $q = 0$; these less symmetric lattices essentially change the relative orientations and positions of the disclinations.

B. Ballistic active force

In the preceding discussions, we have established that an active particle, whether it is a disclination or not, always carries a collection of defects in its random motion. These defects essentially reflect the localized lattice distortion near the active particle. One may wonder if such a scenario of a randomly wandering dressed active particle is also true in its ballistic motion especially when it reaches a high speed. In crystalline materials, fast moving defects can use their kinetic energy to create new defect structures. [54] A defect at high speed is also able to overcome obstacles such as precipitated particles or other defects lying across its path. [55] However, it is a challenge to accelerate a disclination or dislocation whose speed is limited by the sound speed in the medium in a way similar to a relativistic particle. [55] Fast speed of defects may be achieved under large stress. Nevertheless, the maximum magnitude of the imposed stress is limited by the yield stress of the material.

Our model system provides a convenient playground to inspect the idea of employing a ballistic active particle to

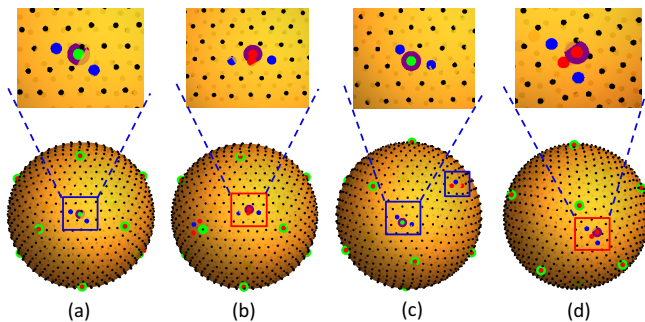


FIG. 3: Typical defect patterns around a ballistic active particle (the large purple dots). An active particle in ballistic motion, either a disclination (c, d) or not (a, b), oscillates between two types of defect patterns as shown in the boxes. The red and blue dots represent 5- and 7-fold disclinations. $\Gamma = 0.002$. $\tilde{f} = 0.1$ (a,b) and 0.2 (c,d). $t/\Delta t = 95000$ (a), 145000 (b), 55000 (c), and 65000 (d). $N = 1002$.

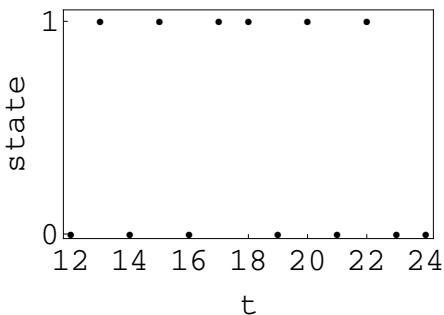


FIG. 4: The defect pattern surrounding an active particle in ballistic motion oscillates between two states: state 0 and state 1 in the boxes in Figs. 3(a) and 3(b), respectively. $\Gamma = 0.002$. $\tilde{f} = 0.1$. t is measured in the unit of $5000\Delta t$. $N = 1002$.

accelerate defects. We regulate the motion of an active particle to be along a uniform direction at constant speed by letting $\hat{u}_i(t)$ be a constant vector and \tilde{f} a constant in Eq.(3). The selected particle subject to such a constant active force is in ballistic motion; the very low level of the noise does not change the ballistic nature of the motion. The speed of the active particle can be controlled by the value for \tilde{f} in Eq.(3). We first consider the case where the active particle is not a disclination and investigate the particle speed ranging from $\tilde{f} = 0.05$ to as high as $\tilde{f} = 0.5$. The previously discussed various defect patterns formed around a randomly moving active particle are observed to uniformly converge to either of the two well-defined topologically neutral defect structures shown in Fig. 3(a) and 3(b), where the active particle is represented by the large purple dot in the box. For convenience, in the following discussions, the defect patterns around the active particle in Fig. 3(a) and 3(b) are named as state 0 and state 1, respectively. In the state 0, the disclinations are organized in the form of 7-4-7, *i.e.*, a string of 7-, 4-, and 7-fold disclinations. The state 1 is in the form of 7-(5-5)-7, where the two 5-fold disclinations

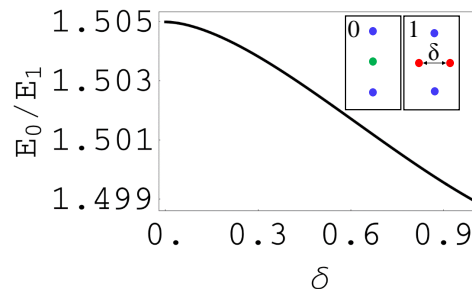


FIG. 5: The ratio of the energies of the two defect patterns around a ballistic active particle. E_0 and E_1 are the energies of the state 0 and the state 1, respectively, as shown in the inset figures (blue dot: 7-fold disclination; green dot: 4-fold disclination; red dot: 5-fold disclination). In these two defect configurations, disclinations of different types are separated by a lattice spacing.

can be very close and are perpendicular to the line of the two 7-fold disclinations. The active particle moves perpendicular to these linear defects. Notably, the originally swelled defect cluster dressing a randomly moving active particle shrinks in the direction of the motion, leading to the wing-like structures.

Simulations show that in the ballistic motion of the active particle the associated defect pattern oscillates between the two states: state 0 (7-4-7) in Fig. 3(a) and state 1 [7-(5-5)-7] in Fig. 3(b). To quantify the oscillation between these two states, we plot Fig. 4 to track the dynamics of the defect pattern around the active particle in time. For the case in Fig. 4 where $\Gamma = 0.002$ and $\tilde{f} = 0.1$, and also for the cases of fast ($\tilde{f} = 0.5$) and slow ($\tilde{f} = 0.05$) active particles, the defect pattern does not prefer either of these two states. Analysis of simulation data suggests that the transition between these two states is random.

These wing-like defect motifs may become unstable with the increase of R/a , where R is the radius of sphere and a is the lattice spacing. $R/a \rightarrow \infty$ in the continuum limit. It has been established theoretically and experimentally that an isolated disclination becomes a linear scar when R/a exceeds about 5. [34–36] The topological charge of the defect in this transformation is preserved. For the topologically neutral wing-like defect, it is speculated based on the case of disclination that it may become a neutral linear defect composed of connecting dislocations. Such a defect called pleat has been experimentally observed in curved crystals confined on capillary bridges. [56]

Here we estimate the energies of the state 0 and the state 1 of the defect pattern around the ballistic active particle from the elasticity theory of topological defects. [34–36] The interaction energy between two disclinations of topological charges q_i and q_j in the spherical crystal is [34]

$$\chi(\beta) \propto q_i q_j \left(1 + \int_0^{\frac{1-\cos\beta}{2}} dz \frac{\ln z}{1-z} \right), \quad (4)$$

where β is the angular distance between the two disclinations. The integral in Eq.(4) can be expressed in terms of the polylogarithm function $Li_n(z) = \sum_{k=1}^{\infty} z^k/k^n$:

$$\int_0^{\frac{1-\cos\beta}{2}} dz \frac{\ln z}{1-z} = -\frac{\pi^2}{6} + Li_2\left(\frac{1+\cos\beta}{2}\right), \quad (5)$$

For small separation β ,

$$\chi(\beta) \propto q_i q_j \left(1 - \frac{1}{4}\beta^2 \ln\left(\frac{4e}{\beta^2}\right) + \mathcal{O}(\beta^3)\right), \quad (6)$$

where e is the Euler's number. Figure 5 shows the ratio of E_0 to E_1 vs δ . E_0 and E_1 are the energies of the state 0 and the state 1, respectively. δ is the separation of the two 5-fold disclinations in the state 1 as shown in the second inset in Fig. 5, measured in the unit of the lattice spacing. We see from Fig. 5 that the value for E_0/E_1 is about 3/2, and it is almost independent of δ . Despite the appreciable energy difference of these two states, their quasi-equal appearance frequency suggests that the energy input to maintain a constant speed of the active particle is much larger than their energy difference.

For a disclinal active particle in its ballistic motion, we also observe that it leaves a net topological charge of +1 in its original site in the form of a 5-7-5 scar [see the defect in the right smaller box in Fig. 3(c)] just like for a randomly moving disclinal active particle. The defect pattern around the active particle in its ballistic motion also oscillates between the state 0 [where the defects are arranged in the form of 7-4-7 as in the large purple dot in the large box in Fig. 3(c)] and state 1 (7-(5-5)-7) as shown in Fig. 3(c) and 3(d), respectively. We vary the speed of the active particle by adjusting the value for \tilde{f} from 0.01 to 0.5. The basic physical picture of dressed active particle and the oscillation between the two states remains over such a broad spectrum for the particle speed.

It is of interest to note that periodic oscillation of defects has been experimentally observed in spherical active nematics, arising from the collective motion of all the active microtubules composing the liquid crystal vesicle. [33] The conformations of the defects are preserved in this process. In contrast, in our spherical crystal system the defect structures are excited by an arbitrarily chosen individual particle. And we observe featured phenomena that are absent in the collective motion in spherical active nematics, including the healing of the defects in the trajectory of the active particle, the scenario of dressed active particle, and the random two-state oscillation of

the surrounding defect pattern.

In our system of electrically charged particles confined on sphere, the emergent defect structures are induced by the motion of a self-propelled active particle in the crystalline order. Similar phenomena also occur in other physical and biological systems, where the motion of an object in an ordered medium can excite emergent structures therein. The specific form of the resulting structures reflects the nature of the ordered medium. For example, a sufficiently fast moving cylinder in fluid can excite the formation of vortices. [57] In crystalline materials, fast moving defects can create new defect structures. [54] A recent study on the collective migration of deformable biological cells shows that individual eukaryotic cells caged in the hexagonal arrangement of cells can deform themselves and exhibit a wiggling motion to escape from the cells cluster. In this process, cells compete for the emergent structure of voids which are formed in the deformation of cells. [58]

IV. CONCLUSION

In summary, simulations show that a moving active particle in spherical crystal is surrounded by localized topological defects, becoming a dressed active particle. As a consequence of the long-range repulsion between particles, the trajectory of the active particle is free of defects. We further observe the random oscillation of a ballistic active particle between two defect states. The nonequilibrium behaviors of spherical crystal excited by a moving active particle involve dynamics of all the particles. We demonstrate that focusing on the structure of topological defects significantly reduces the degree of freedom of the system, and the physical picture of dressed active particle emerges. This work opens the promising possibility of introducing activity to efficiently engineer crystallographic defects for desired materials properties.

Acknowledgement

This work was supported by the SJTU startup fund under Grant No. WF220441904 and the award of the Chinese Thousand Talents Program for Distinguished Young Scholars under Grant No. 16Z127060004.

-
- [1] T. Vicsek, A. Czirók, E. Ben-Jacob, I. Cohen and O. Shochet, *Phys. Rev. Lett.*, 1995, **75**, 1226.
[2] R. Zwanzig, *Nonequilibrium Statistical Mechanics*, Oxford University Press, USA, 2001.
[3] M. Marchetti, J. Joanny, S. Ramaswamy, T. Liverpool,

- J. Prost, M. Rao and R. A. Simha, *Rev. Mod. Phys.*, 2013, **85**, 1143.
[4] R. Ni, M. A. C. Stuart and M. Dijkstra, *Nat. Commun.*, 2013, **4**, 2704.
[5] J. K. Parrish and W. M. Hamner, *Animal Groups in*

- Three Dimensions: How Species Aggregate*, Cambridge University Press, 1997.
- [6] J. Toner and Y. Tu, *Phys. Rev. E*, 1998, **58**, 4828.
- [7] A. Zöttl and H. Stark, *arXiv preprint arXiv:1601.06643*, 2016.
- [8] H.-P. Zhang, A. Beer, E.-L. Florin and H. L. Swinney, *Proc. Natl. Acad. Sci. U.S.A.*, 2010, **107**, 13626–13630.
- [9] W.-J. Rappel, A. Nicol, A. Sarkissian, H. Levine and W. F. Loomis, *Phys. Rev. Lett.*, 1999, **83**, 1247.
- [10] X. Trepát, M. R. Wasserman, T. E. Angelini, E. Millet, D. A. Weitz, J. P. Butler and J. J. Fredberg, *Nat. Phys.*, 2009, **5**, 426–430.
- [11] S. Wang and P. G. Wolynes, *Proc. Natl. Acad. Sci. U.S.A.*, 2011, **108**, 15184–15189.
- [12] S. Zhou, A. Sokolov, O. D. Lavrentovich and I. S. Aranson, *Proc. Natl. Acad. Sci. U.S.A.*, 2014, **111**, 1265–1270.
- [13] I. S. Aranson and L. S. Tsimring, *Rev. Mod. Phys.*, 2006, **78**, 641.
- [14] V. Narayan, S. Ramaswamy and N. Menon, *Science*, 2007, **317**, 105–108.
- [15] B. M. Mognetti, A. Šarić, S. Angioletti-Uberti, A. Cacciuto, C. Valeriani and D. Frenkel, *Phys. Rev. Lett.*, 2013, **111**, 245702.
- [16] W. F. Paxton, K. C. Kistler, C. C. Olmeda, A. Sen, S. K. St. Angelo, Y. Cao, T. E. Mallouk, P. E. Lammert and V. H. Crespi, *Journal of the American Chemical Society*, 2004, **126**, 13424–13431.
- [17] S. Henkes, Y. Fily and M. C. Marchetti, *Phys. Rev. E*, 2011, **84**, 040301.
- [18] N. H. Nguyen, D. Klotsa, M. Engel and S. C. Glotzer, *Phys. Rev. Lett.*, 2014, **112**, 075701.
- [19] M. Spellings, M. Engel, D. Klotsa, S. Sabrina, A. M. Drews, N. H. Nguyen, K. J. Bishop and S. C. Glotzer, *Proc. Natl. Acad. Sci. U.S.A.*, 2015, **112**, E4642–E4650.
- [20] F. Schweitzer and J. Farmer, *Brownian Agents and Active Particles*, Springer, 2007.
- [21] T. Vicsek and A. Zafeiris, *Phys. Rep.*, 2012, **517**, 71–140.
- [22] P. Tierno, R. Golestanian, I. Pagonabarraga and F. Sagués, *Phys. Rev. Lett.*, 2008, **101**, 218304.
- [23] J. Palacci, S. Sacanna, A. P. Steinberg, D. J. Pine and P. M. Chaikin, *Science*, 2013, **339**, 936–940.
- [24] J. Palacci, S. Sacanna, A. Vatchinsky, P. M. Chaikin and D. J. Pine, *J. Am. Chem. Soc.*, 2013, **135**, 15978–15981.
- [25] R. Zhang, D. A. Walker, B. A. Grzybowski and M. Olvera de la Cruz, *Angew. Chem. Int. Ed.*, 2014, **126**, 177–181.
- [26] A. Chaudhuri, B. Bhattacharya, K. Gowrishankar, S. Mayor and M. Rao, *Proc. Natl. Acad. Sci. U.S.A.*, 2011, **108**, 14825–14830.
- [27] T. Sanchez, D. T. Chen, S. J. DeCamp, M. Heymann and Z. Dogic, *Nature*, 2012, **491**, 431–434.
- [28] X.-Q. Shi and Y.-Q. Ma, *Nat. Commun.*, 2013, **4**, 3013.
- [29] L. Giomi, M. J. Bowick, X. Ma and M. C. Marchetti, *Phys. Rev. Lett.*, 2013, **110**, 228101.
- [30] R. Sknepnek and S. Henkes, *Phys. Rev. E*, 2015, **91**, 022306.
- [31] V. Schaller and A. R. Bausch, *Proc. Natl. Acad. Sci. U.S.A.*, 2013, **110**, 4488–4493.
- [32] L. Penrose, *Nature*, 1965, **205**, 544–546.
- [33] F. C. Keber, E. Loiseau, T. Sanchez, S. J. DeCamp, L. Giomi, M. J. Bowick, M. C. Marchetti, Z. Dogic and A. R. Bausch, *Science*, 2014, **345**, 1135–1139.
- [34] M. Bowick, A. Cacciuto, D. R. Nelson and A. Traveset, *Phys. Rev. Lett.*, 2002, **89**, 185502.
- [35] A. Bausch, M. Bowick, A. Cacciuto, A. Dinsmore, M. Hsu, D. Nelson, M. Nikolaidis, A. Traveset and D. Weitz, *Science*, 2003, **299**, 1716–1718.
- [36] M. J. Bowick, A. Cacciuto, D. R. Nelson and A. Traveset, *Phys. Rev. B*, 2006, **73**, 024115.
- [37] D. Struik, *Lectures on Classical Differential Geometry*, Dover Publications, 2nd edn, 1988.
- [38] P. M. Chaikin and T. C. Lubensky, *Principles of Condensed Matter Physics*, Cambridge Univ Press, 2000, vol. 1.
- [39] J. M. Kosterlitz and D. J. Thouless, *J. Phys. C: Solid State Phys.*, 1973, **6**, 1181.
- [40] B. Halperin and D. R. Nelson, *Phys. Rev. Lett.*, 1978, **41**, 121.
- [41] D. R. Nelson and B. Halperin, *Phys. Rev. B*, 1979, **19**, 2457.
- [42] A. Young, *Phys. Rev. B*, 1979, **19**, 1855.
- [43] K. J. Strandburg, *Rev. Mod. Phys.*, 1988, **60**, 161.
- [44] D. L. Caspar and A. Klug, Cold Spring Harbor Symposia on Quantitative Biology, 1962, pp. 1–24.
- [45] B. Szabo, G. Szöllösi, B. Gönci, Z. Jurányi, D. Selmecki and T. Vicsek, *Phys. Rev. E*, 2006, **74**, 061908.
- [46] G. Szamel, E. Flenner and L. Berthier, *Phys. Rev. E*, 2015, **91**, 062304.
- [47] P. Kloeden and E. Platen, *Numerical Solution of Stochastic Differential Equations*, Springer, 1995.
- [48] T. Ihle, *Eur. Phys. J. Special Topics*, 2014, **7**, 1293–1314.
- [49] S. Kim and S. Karrila, *Microhydrodynamics: Principles and Selected Applications*, Dover, New York, 2005.
- [50] A. Pérez-Garrido and M. Moore, *Physical Review B*, 1998, **58**, 9677.
- [51] T. Erber and G. Hockney, *Journal of Physics A: Mathematical and General*, 1991, **24**, L1369.
- [52] Z. Yao and M. Olvera de la Cruz, *Phys. Rev. E*, 2014, **90**, 062318.
- [53] Z. Yao and M. Olvera de la Cruz, *Proc. Natl. Acad. Sci.*, 2014, **111**, 5094.
- [54] N. Mott and F. Nabarro, *Report on Strength of Solids*, Physical Society, London, 1948, pp. 1–19.
- [55] A. H. Cottrell, *Dislocations and Plastic Flow in Crystals*, Clarendon Press, 1965.
- [56] W. T. Irvine, V. Vitelli and P. M. Chaikin, *Nature*, 2010, **468**, 947–951.
- [57] L. D. Landau and E. M. Lifshitz, *Fluid Mechanics*, Butterworth, 1987.
- [58] J. Löber, F. Ziebert and I. S. Aranson, *Sci. Rep.*, 2015, **5**, 9172.